A Microfluidic Serial Dilutor (MSD): Design Optimization and Application to Tuning of Liposome Nanoparticle Preparation

Huanhuan Shi[a, *], Zhihao Xie[a], Yu Cao[a], Yali Zhao[b, *], Congxuan Zhang[a], Zhen Chen[a, *], Nuno M Reis[c], Zhengchun Liu[d]

[a]Department of Biomedical Engineering, School of Measuring and Optical Engineering, Nanchang Hangkong University, Nanchang, Jiangxi 330063, People's Republic of China

[b]The Fourth Hospital of Changsha, Changsha Hospital of Hunan Normal University, Changsha, 410006, PR China

[c]Department of Chemical Engineering and Centre for Biosensors, Bioelectronics and Biodevices (C3Bio), University of Bath, Claverton Down, Bath BA2 7AY, UK

[d]Hunan Key Laboratory for Super Microstructure and Ultrafast Process, Department of Electronic Information Science and Technology, School of Physics and Electronics, Central South University, Changsha, 410083, People's Republic of China

*Corresponding author: shihuanhuancsu@126.com, zhaoyali-789@163.com, dr_chenzhen@163.com

Abstract

Dilution of a sample over several orders of magnitude in concentration is a routine procedure in many analytical, bioanalytical, diagnostics, and formulation laboratories. Microfluidics offer the opportunity to automate the dilution procedure with many successful designs to be found in literature, yet fast microfluidic generation of a dilution series over several orders of magnitude remains so far unaddressed. This study realized a microfluidic serial dilutor (MSD) having up to 4 outlets and able to generate fast a serial dilution of a sample up to 4 orders of magnitude. The core design based on a cascade dilution of sample to diluent in a 1:10 volume ratio was fully characterized experimentally and using Computational Fluid Dynamics (CFD). The MSD was interfaced with a new absorbance measuring device based on a laser diode and spectral sensor, which enabled evaluating the dilution performance and confirming the effectiveness of the design. The MSD was applied to the synthesis of liposome nanoparticles by solvent diffusion method, enabling fine-tunning of synthesis of a popular drug and vaccine delivery microcarrier on a wide range of sizes by simply adjusting the flow rate and flow rate ratio. The MSD design showed to be simple, reliable, with operation at reduced pressure drops, and delivery of highly reproducible results.

Keywords: *Microfluidic dilutor; Micro-mixing; Absorbance measurement; liposome nanoparticle; Tunable Fabrication*

1. Introduction

As the carrier of encapsulated drugs, nanoparticles can realize controlled and sustained release of drugs(de Almeida et al., 2021; Tang et al., 2021). Vaccines represented by mRNA have established a reliable barrier to human health. mRNA vaccines are lipid nanoparticles (NPs) that contain mRNA internally(Chaudhary et al., 2021; Tenchov et al., 2021). Currently, the liposomal-based mRNA vaccines were fabricated by pumping the lipid solution and mRNA solution through different channels and mixing the two solutions using a jet mixer under high pressure(Hou et al., 2021; Kim et al., 2021). To meet the needs of mass production, hundreds of static mixers are parallelized for continuous synthesis, but if the vaccine formulation needs to be changed, the entire production line should be adjusted accordingly(Liu et al., 2022; Prakash et al., 2022). Additionally, as the virus mutates, the vaccine formulations and the fabrication of nanocarriers should be adjusted rapidly, so achieving a continuous synthesis of liposome nanoparticles with tunable formulations seems to remain a need and challenge.

Compared to the traditional mass production mode, microfluidic technology can process a microliter volume of sample (or smaller), with lower production cost and shorter production time(Shi et al., 2021; Shi et al., 2019b). The quality of nanoparticles (such as size, shape and surface properties, structure, etc.) could be precisely controlled through fast and thorough mixing, mass transfer, and accurate control reaction conditions(Shi et al., 2020b; Suzuki et al., 2021). The high throughput microfluidic mixer can be realized by multi-channel parallel amplification, which is beneficial to large-scale industrial production(Maeki et al., 2018). However, when the microfluidic chip design is fixed, there is little control over the produced liposome nanoparticles except for the flow rate. If the output concentration can be adjusted on the same microfluidic chip (the adjustment range is not limited to one order of magnitude but across orders of magnitude), it is possible to provide a large adjustable range for the development and formulation optimization of liposome nanomedicine screening.

Excitingly, Whitesides *et al*. (Jeon et al., 2000) proposed the concept of the classic "Christmas tree model" microfluidic concentration gradient based on the principle of laminar diffusion mixing at low Reynolds number, which was still in use today(Lee and Fu, 2018). Through the automatic diffusion of mixed flow in a microchannel, Microfluidic Concentration Gradient (MCG) technology can achieve accurate control of output concentration, which was mainly used for high-throughput drug screening(Khoo et al., 2018; Lim and Park, 2018), chemical toxicity analysis(Gonzalez-Suarez et al., 2018), chemotactic studies(Berendsen et al., 2020; Roggo et al., 2018) and material synthesis(Hu et al., 2020). The "Christmas tree model" MCG also has some disadvantages such as long channel length and long gradient formation

time(Rismanian et al., 2019). Some simple concentration gradient designs have been reported. Shi *et al.*(Shi et al., 2019a) proposed a multi-inlets MCG for the concentration gradient formation of antibacterial drugs. At the flow rate of 2280 μl/min, the linear concentration gradient can be realized in a few seconds according to the fast micro-mixing principle, and the gradient shape is independent of the flow rate. Ahrar *et al.*(Ahrar et al., 2014) adopted the valve-driven circulatory mixing to construct a new structure to store each stage of the dilution process for the 7-stage series of 1 : 1 dilutions. Wan *et al.*(Wan and Yin, 2018) designed a tunable and quantitative serial dilution chip analogous to an electrical circuit. The dilution chip was integrated into a miniaturized microfluidic electrochemical platform for verification. Avesar *et al.*(Avesar et al., 2018) reported a microfluidic dilution chip for generation of a high resolution chemical gradient spanning 200 nanoliter wells for the study of yeast cell metabolic gene regulation.

However, concentration gradient within one order of magnitude may not be sufficient to regulate processes like the preparation of liposome nanoparticles. It is necessary to develop concentration dilution chips that across orders of magnitude. At present, only a few studies have reported the dilution of samples across orders of magnitude with microfluidic chip. Kim *et al.*(Kim et al., 2018) developed a N-fold (N=2-10) serial dilution centrifugal microfluidic device. The pre-programmed operation of the valves was used to control the flow within the microchannel. Kim *et al.*(Kim et al., 2008) proposed a continuous ten-fold dilution and linear dilution microfluidic chip network design based on the Tesla mixing channel and equivalent circuit design principle. The fluorescein solution and cytotoxicity test were used to dilution performance evaluation, respectively. Sugiura *et al.*(Sugiura et al., 2010) developed a microfluidic tandem dilution chip to study the cell response to drugs in a wide range of drug concentrations. The dilution microfluidic network was eventually able to dilute drug concentration across 6 orders of magnitude. The injection and culture of cells took about 6-12 hours, and the injection process of medium and drug solution requires 5-20 kPascal pressure, which is highly resistant to pressure on the chip. Horrocks *et al.*(Horrocks et al., 2013) found that cross-order dilution using microfluidic chips is a good tool for single-molecule measurements of transient biomolecular complexes. The proposed microfluidic device can dilute the sample by 100,000 times rapidly, can observe unstable biological complexes before dissociation. However, this device can only produce the final diluted product. The intermediate diluted product was not available. Similarly, Zijlstra *et al.*(Zijlstra et al., 2017) designed a microfluidic chip capable of generating five orders of magnitude concentration gradients for single-molecule spectra of low-affinity biomolecular complexes, which can dilute concentrated samples in milliseconds, but the problem is that there is a large pressure drop at the inlet, up to 10-20 kPascal. At present, the shortcomings of dilution chip across orders of magnitude are

the complicated microfluidic networks, which leads to huge pressure drop and longer gradient formation time, etc., or it is difficult to flexible adjust the concentration types.

Therefore, it is necessary to develop a microfluidic concentration dilutor across orders of magnitude with simple structure, less pressure drop, and flexible adjustability. In this work, ten-fold dilution of samples through one-to-nine non-equal volume mixing were achieved, high-performance micro-mixing channels was introduced to improve the mixing efficiency and shorten the mixing channel length. Serial ten-fold dilution of sample was realized by connect those mixing structures in series. The flexible adjustability of outlet concentrations was investigated by computational fluid dynamics (CFD) simulations and fluorescence flow experiments. A real-time sample absorbance measurement platform was constructed for dilution performance verification. The microfluidic dilutor was applied to the controllable preparation of liposome nanoparticles, which proved its application potential for formulation optimization of nanoparticle synthesis.

2. Methods and experimental

2.1 Regents and apparatus

Sylgard 184 and Silicone elastomer curing agent were purchased from Dow Chemical for Polydimethylsiloxane (PDMS)-glass chip fabrication. Sodium fluorescein was purchased from 9ding chemicals, Shanghai, China. Soybean lecithin and cholesterol (AR, >95%) was obtained from Yuanye Biology, China, methanol (HPLC) was purchased from Daomao chemicals, Tianjin, China. Teflon pipe (1/16) and stainless-steel pipe joint were purchased from Beionfluid, Shanghai, China. Digital microscope (Magnification 500×, pixels 2 million) was obtained from Andonstar, China. Olympus microscope (BX41-32PO2) was used to observe the microchannel of PDMS-glass chip. Syringe pumps were obtained from LongerPump and Leadfluid China. Liposome nanoparticles were synthesized through the mixing of water and the mixture of soybean lecithin and cholesterol into the micro dilutor channel. Particle Sizer and Zeta Potential Analyzer is adopted to characterize the liposome nanoparticles (90Plus PALS, Brookhaven Instruments, USA). Laser diode (480nm) was purchased from Hamamatsu Electronics of Japan, Multichannel spectral sensor (AS7341, AMS company, which has been reported for spectral measurement(Baumker et al., 2021)) was obtained from Shenzhen Fengtai Electronics, China. Arduino Microprogrammed Control Unit (MCU, seeeduino xiao) was obtained from Seeed studio Company. Different concentrations of sodium fluorescein were characterized with fluorospectrophotometer (F98, Lengguang Company, Shanghai, China (Gain 450 v)) and ultraviolet specrophotometer (UV-2550, Shimadzu, Japan), respectively.

2.2 Design principle and CFD simulations details

Under the assumption of perfect mixing, the concentration at outlet could be determined by the initial concentration of sample and diluent, and their volume flow rate of Q. If the $C_{diluent}$ (C means concentration) was regarded as 0, and C_{sample} was regarded as 1, and the desired C_{out} was set 0.1, then $Q_{sample}/Q_{diluent}$ must equal to 9:1 (Fig. 2a)

$$C_{out}=\frac{Q_{Sample}C_{Sample}+Q_{diluent}C_{diluent}}{Q_{Sample}+Q_{diluent}} \quad (1)$$

Based on this, the serial concentration dilution chip that dilute the sample over five orders of magnitude was designed. Inlet 1 and inlet 2 were used to respectively load sample and diluent at flow rate ratio of 1:9, thus C_1 at outlet 1 would be 0.1. Four dilution structures were adopted to continuously dilute sample, and inlet 3 was utilized to provide a common diluent flow rate (Fig. 2b). The CFD simulation was conducted with Fluent software that was similar to our previous work(Shi et al., 2019a).

2.3 Microfluidic chip fabrication and construction of absorbance measurement device

Microfluidic dilution chip fabrication: The microchannel design is transferred to the photoresist by blocking a specific area (mask) in the photolithography process. The graphic design on the mask is transferred to the silicon wafer of SU-8 photoresist of a certain thickness by using the photolithography technology, including pretreatment, homogenizing, pre-baking, exposure, post-baking, developing, and hard film. After pouring PDMS on the mold, the PDMS was solidified, and then the stripped PDMS substrate was bonded with glass to form a microfluidic chip (Fig. 1b). The chip in this work was placed on horizontal plane, gravitational influences on laminar flows inside the microchannel second only to best condition (aligned with the gravitational field). In the subsequent optimization design, if the flow direction can be unified with the gravity direction, the influence of gravity will be minimized(Giorello et al., 2020).

Absorbance measurement device: this device was constructed for real-time monitoring of solution concentrations. It was consisted of a laser diode (480 nm) and a multi-channel spectrum sensor that were placed on the both sides of the microcuvette. According to the Lambert-Beer law, there is a linear relationship between absorbance and solution concentration. Therefore, the absorbance of the solution is calculated using the incident light intensity and the detected light intensity. The device has been fully verified on the microcuvette and then used to monitor the diluted solution collected in different microcuvette. The light intensity data collected by the spectral sensor are transmitted to the computer for display and recording by MCU.

2.4 Synthesis of liposome nanoparticles with microfluidic chip

The solvent diffusion method was used for liposome nanoparticle preparation(Sun et al., 2015; Yuan et al., 2013; Zhao et al., 2018). Soybean lecithin (0.01M) and cholesterol (0.002M) were dissolved in 20mL methanol as liquid A. Another two tubes of water as liquid B and C. 1ml liquid A was loaded into a 1ml syringe (diameter= 0.7mm) as sample connected to inlet 1, and another two 20 mL liquid B and C were loaded into two 20 ml syringes (diameter =2.1mm) as buffers connected to inlet 2 and inlet 3 respectively. The 1ml syringe (liquid A) and one 20 ml syringe (liquid B) were driven by the same pump. Since the inner diameter ratio of 1ml and 20ml syringe is 1:3, the volume-flow rate ratio is 1:9 under the action of the same driving force (30, 60 μl/min). Another pump was used to adjust the flow rate of inlet 3 individually (180, 330, 600, 800 μl/min). To closer to the CFD settings, the length of the inlets pipe was adjusted accordingly try to make the liquid reach three inlet ports at the same time. The tuning of liposome nanoparticles fabrication can be achieved flexibly by increasing the flow rate of inlet 1, 2 and 3, or adjusting the flow rate of inlet 3 alone (Fig. 1a).

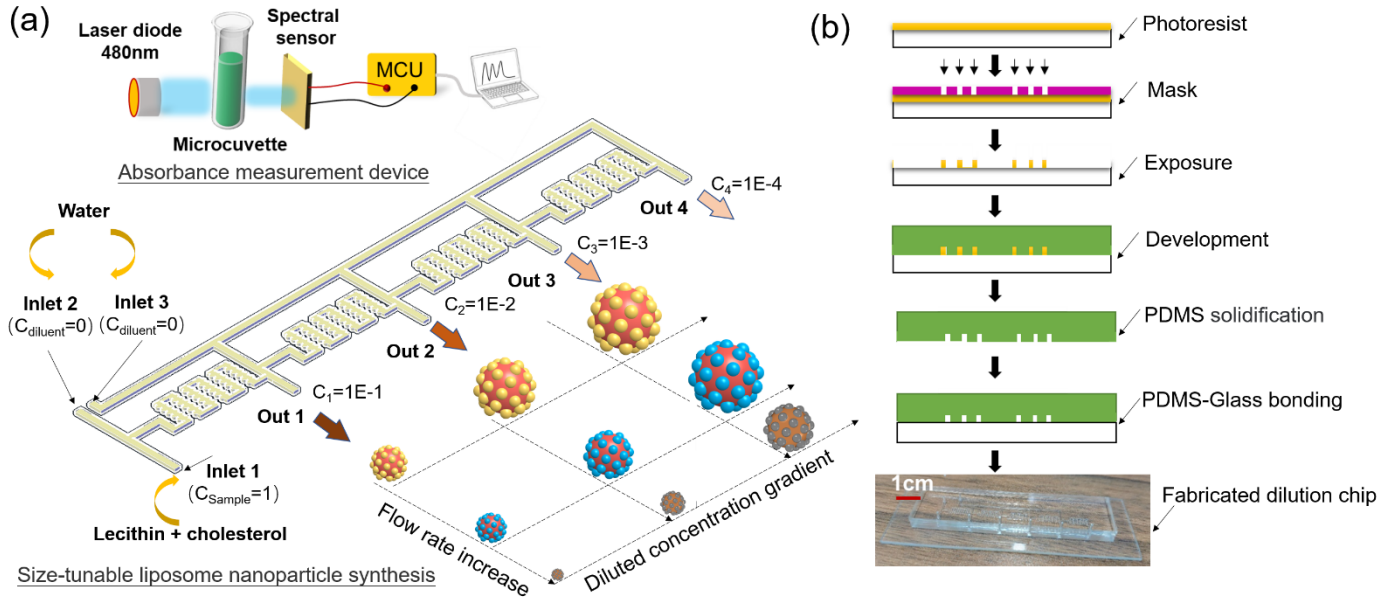

Fig. 1 (a) Illustration of size-tunable liposome nanoparticle synthesis using the dilution chip over orders of magnitude and absorbance measurement device for concentration verification; (b) Fabrication process of PDMS-glass dilution chip.

3. Results and discussion

3.1 CFD simulations and validation of the micro-dilutor

To achieve concentration dilution of the sample over orders of magnitude, a tenfold dilution of the sample is first required with the most used T-shaped mixer (as shown in Fig. 2a). A tenfold dilution of the sample could be only achieved when the volume ratio of diluent and sample was 9:1. When the inlet cross-

sectional areas of diluent and sample are equal, the inlet flow rate only needs to be adjusted to 9:1 to achieve the volume ratio of 9:1 (Fig. 2a(i)). If the two inlet flow rates are equal, the inlet cross-sectional area needs to be adjusted to 9:1(Fig. 2a(ii)). According to the concentrations at the outlet nodes ((Fig. 2a(iv))), except for the two situations above, other T-mixer designs cannot achieve ten-fold dilution (Fig. 2a(iii)). However, it is difficult to maintain the accurate cross-sectional area ratio (9:1) all along the tubes for the actual experiment. It is simpler to set the inlet cross-sectional area to be the same and the inlet flow rate ratio to be 9:1, thus ten times dilution can be achieved by unequal flow rate mixing (Fig. 2a(v)).

In addition, the influence of the mixing efficiency of the mixing channel should also be considered, because the structure needs to be successively connected for serial dilution. If the mixing of the previous stage is not sufficient, the concentration of sample for the second dilution structure is bound to be inaccurate, which will affect the subsequent dilution performance step by step. Moreover, better mixing using a shorter mixing channel will simplify the dilution structure. Therefore, the improved serpentine mixing channel with lateral structure reported in our previous work was introduced(Shi et al., 2020a).

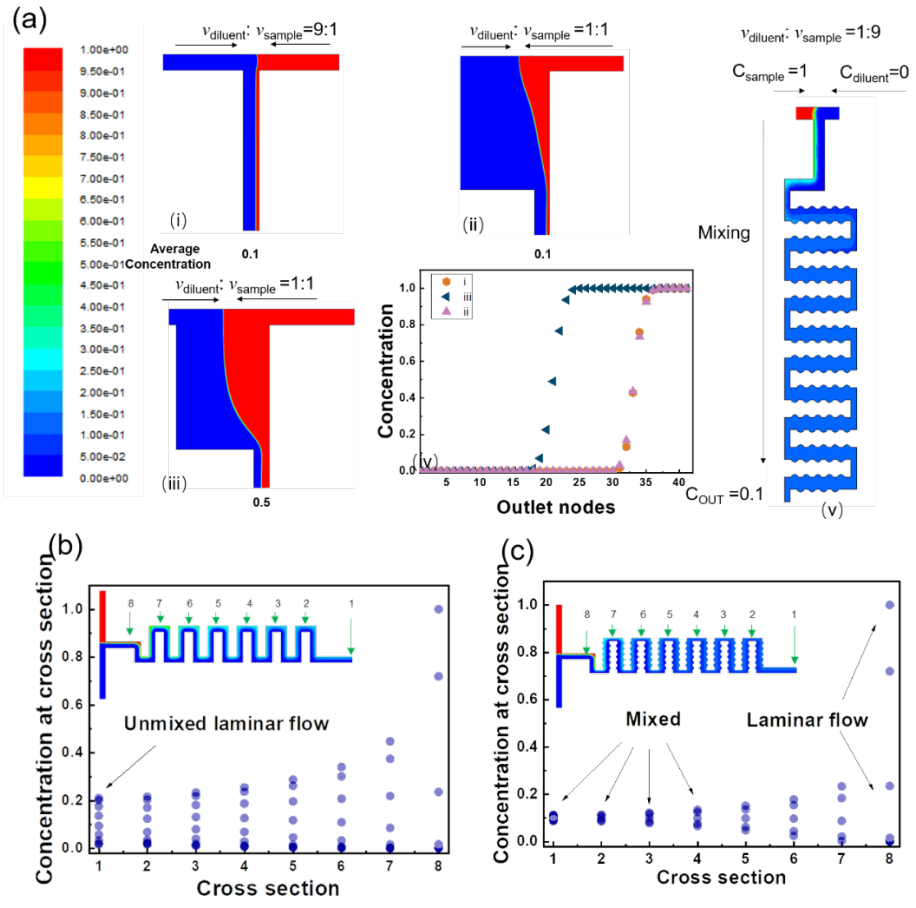

Fig. 2 (a) tenfold dilution of sample solution using a T-mixer: (i) Flow rate of v_{buffer}: v_{sample}=9: 1. (ii) Inlet cross section of S_{buffer}: S_{sample}= 9: 1. (iii) Inlet channel width of W_{buffer}: W_{sample}= 9: 1. (iv) Concentrations at outlet nodes for the three situation above. (v) Tenfold dilution achieved by unequal flow rate mixing using the improved serpentine channel. (b)

Mixing performance comparison of the ordinary and the improved serpentine channel.

As shown in Fig. 2b and 2c, under the same set of inlet conditions, the mixing performance of the ordinary and the improved serpentine mixing channel were compared in terms of the concentration distribution of the nodes on some selected cross sections. The concentration node distribution of the ordinary serpentine mixed channel is more dispersed, while that of the improved serpentine mixed channel is more concentrated, which means that the mixing effect achieved by the improved microchannel at each cross-section is better than that of the ordinary type (for unequal volume mixing, 9: 1).

Based on the above results, five dilution structures were connected in series (Fig. 1a). The output of the pervious mixing (completely mixed) will be adopted as the input sample of the next dilution structure. At the same time, a common dilution channel is introduced on the side for the subsequent step-by-step dilution process. Therefore, if the tenfold dilution was achieved at the first stage, and its output is further diluted tenfold, and so on, multistage sample dilution can theoretically be achieved.

After the serial dilution chip was constructed, the optimal flow rate conditions need to be further investigated by CFD simulations. Since the concentration of outlet 1 must be 0.1, therefore, according to the theory of equation (1), the flow rate ratio of inlet 1 and inlet 2 was fixed (1:9). So, the flow rate of inlet 1 and inlet 2 was set at 0.055 m/s and 0.5m/s, respectively. And the flow rate of the inlet 3 was changed from 0.5 to 0.9 m/s. As shown in Fig. 3a, as the flow rate ratio of the inlet 3 to inlet 2 increases from 1:1 to 9:5, the diluted sample concentration shape at the outlets was closer to the dilute purpose. But further increasing the flow rate of inlet 3 would result in higher pressure for the liquid drive device. The best result was achieved under the condition of the 9:5 ratio of flow rate of inlet 3 to inlet 2 (Table 1).

To achieve precision tuning of inlet 3 flow rate, the flow rate of inlet 1 and inlet 2 were set 0.03m/s and 0.27 m/s, respectively. The flow rate of inlet 3 was further fine-tuned from 0.5-0.6m/s (Table 1). As shown in Fig. 3b, when the flow rate of inlet 3 was 0.57 m/s, the dilution result was very close to the purposed of five orders of concentration magnitude dilution. By the way, the pressure drops under these conditions are very small and can meet the actual requirement.

In theory, continuous dilution of liquid can be achieved through the infinite connections of dilution structure, but it also needs to increase the flow rate of inlet 3. Since it is more difficult for the liquid to enter the subsequent dilution structure, the possibility of such dilution only exists in theory. In fact, under the relatively common flow rate, 3 orders of concentration magnitude dilutions are already the limit for this chip. Otherwise, it would have a great requirement for the bonding of the PDMS-glass chip and the injection of a syringe pump.

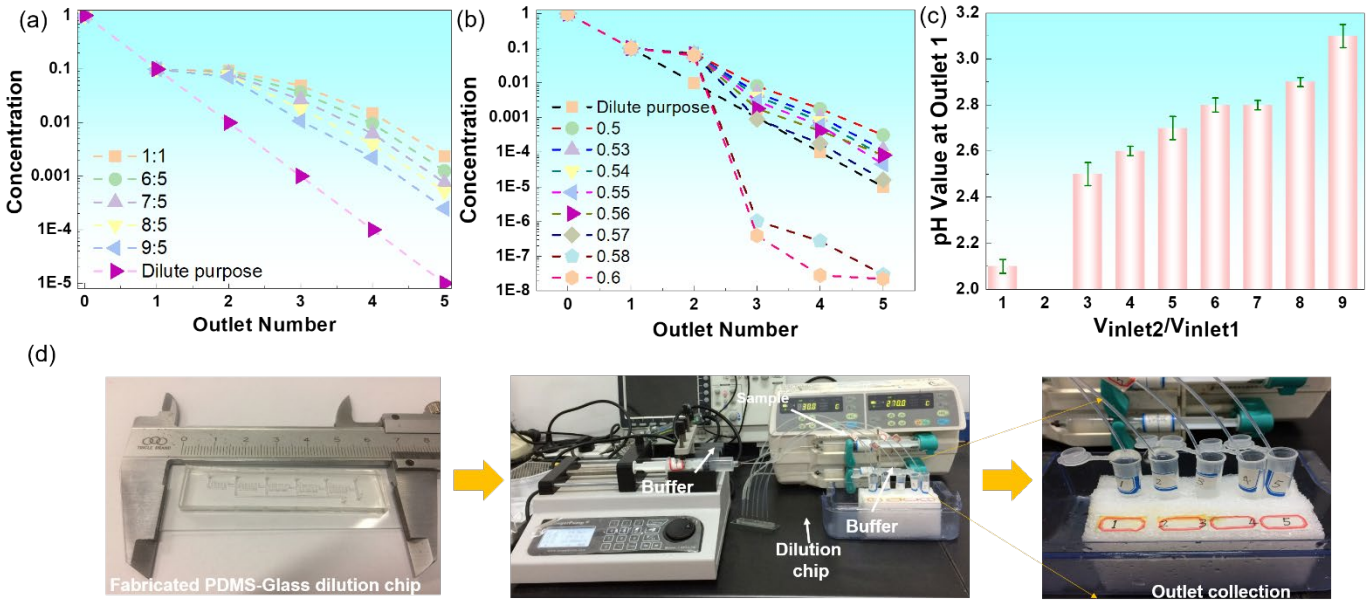

Fig. 3 (a) Dilution results at outlets as the flow rate ratio of the inlet 3 to inlet 2 increases from 1:1 to 9:5 (inlet 1 =0.055m/s and inlet 2 =0.5m/s). (b) Dilution results at outlets as the flow rate the inlet 3 increases from 0.5 to 0.6m/s (inlet 1 =0.03m/s and inlet 2 =0.27m/s). (c) pH value of the solution at outlet 1 under various v_{inlet2}/ v_{inlet1}. (d) pH dilution experiment setups.

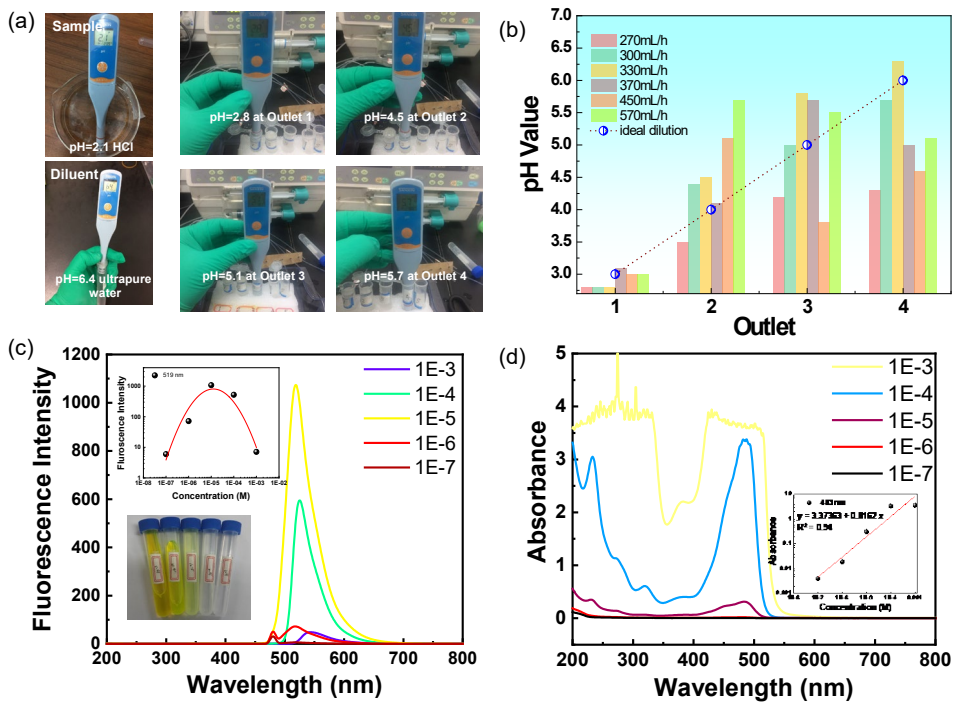

Table 1 Inlet velocity (m/s)

Inlet 1	Inlet 2	Inlet 3
0.055	0.5	0.5
0.055	0.5	0.6
0.055	0.5	0.7
0.055	0.5	0.8
0.055	**0.5**	**0.9**
0.03	0.27	0.5
0.03	0.27	0.53
0.03	0.27	0.54
0.03	0.27	0.55
0.03	0.27	0.56
0.03	**0.27**	**0.57**
0.03	0.27	0.58
0.03	0.27	0.6

Fig. 4 (a) Pictures of pH dilution of HCl (pH=2.1) at outlet1-outlet4. (b) pH dilution of HCl (pH=2.1) at outlet1-outlet4 under various flow rate of inlet 3. (c) Fluorescence intensity of sodium fluorescein over orders of concentrations (1e-3~1e-7) M. (d) Absorbance of sodium fluorescein over orders of concentrations (1e-3~1e-7) M.

According to the previous CFD simulations, a PDMS-glass microfluidic gradient dilution chips were

fabricated by soft lithography and used for pH dilution experiments as shown in Fig. 3d. As we know, the pH value is a logarithmic value that represents the concentration of hydrogen ions in a solution. Therefore, if the proposed chip can be used to dilute hydrogen ion concentration over orders of magnitude (the results can be easily measured by pH meter), the dilution performance of the chip would be preliminary confirmed.

First, the ten-fold dilution was verified by micro-mixing of diluent and sample at a flow rate ratio of 9:1 at outlet 1. The flow rate of the sample was fixed at 30 ml/h at inlet 1, the flow rate of the diluent at inlet 2 was set to 30, 120, 150, 180, 210, 240, 270 ml/h, respectively. The sample used in this experiment is hydrochloric acid solution with pH of 2, and the buffer is ultra-pure water with pH of 6.4. Theoretically, when the flow rate ratio of inlet 2 to inlet 1 is 9:1, the solution of hydrochloric acid with pH of 2 can be diluted ten times to become a solution of hydrochloric acid with pH of 3. As shown in Fig. 3c, with the increase of the flow rate ratio of inlet 2 to inlet 1, the pH value of the solution at outlet 1 increases gradually. When the flow rate ratio of inlet 2 to inlet 1 is 9 (flow rate of inlet 2=270 ml/h), the pH value of the solution at outlet 1 is around 3, which is consistent to the theoretical value and verified the design concept of dilution based on unequal flow rate mixing in Fig. 2a.

Then, in the subsequent tests, the flow rate of inlet 1 and inlet 2 was set 30 and 270 ml/h (1:9), and the flow rate of inlet 3 was adjusted in turn (270, 300, 330, 370, 450 and 570 ml/h) to measure the pH value of the solution obtained from outlet 1-5. As shown in Fig. 4a, and 4b, the best dilution results that is the close to the ideal dilution was achieved when the flow rate of inlet 3 is set at 330 ml/h, which is slightly different from the CFD simulation result (CFD indicate that inlet 3=0.57m/s for the best dilution results). The above results prove that the proposed chip has samples dilution ability over orders of concentration magnitude, but for solutions with different concentrations and viscosity, the optimal inlet flow rates need to be screened for the best dilution results.

Moreover, to characterize the process of concentration gradient more accurately, liquid flow with fluorescence or dye is a good choice for concentration characterization. Ascribe to the large range of concentrations, the concentration is not proportional to the fluorescence intensity. When the fluorescent substance concentration is too low, the fluorescence intensity is low. But if the concentration is too high, the incident light is difficult to penetrate the liquid, also can lead to the fluorescence absorbed by the liquid itself, resulting in low fluorescence intensity. This indicates that fluorescence intensity is more suitable for concentration gradient characterization within one order of magnitude, but not for concentration across multiple orders of magnitude (Fig. 4c). As shown in Fig. 4d, the concentrations of solution are directly proportional to the absorbance, especially in the range of (1e-4 ~ 1e-7) M, the linearity is about 94%.

Therefore, it is necessary to construct a device capable of real-time measurement of solution absorbance at outlets for concentration characterization.

3.2 Construction of absorbance measurement device for real-time dilution performance verification

According to Lambert-Beer law, the absorbance is directly proportional to the concentration of the light-absorbing substance.

$$\text{Absorbance: } A = -\lg T = -\lg(I/I_0) = \varepsilon CL \qquad (2)$$

The absorbance (A) is proportional to the concentration (C) of the absorbent substance and the thickness (length, L) of the absorption layer. I_0 is the intensity of incident light; I is the intensity of transmitted light; T is the transmittance. The concentration across orders of magnitude cannot be determined by fluorescence intensity, but can be determined by absorbance. To realize the purpose of real-time analysis, a miniaturized absorbance device is needed for the dilution performance evaluation.

A micro cuvette was used to collect the liquid at the outlet, and the collected liquid was irradiated by a 480 nm laser diode. The light that penetrates the liquid was analyzed by a spectral sensor (Fig. 5a). Various concentrations of sodium fluorescein were irradiated by the 480 nm laser diode as shown in Fig. 5b. The light intensity measured by the spectral sensor showed the light of 480 nm was absorbed by the sodium fluorescein solution with the increase of its concentrations. Some weak fluorescent lights at 512 nm induced by incident laser light were also detected.

As the concentration of sodium fluorescein increases, the intensity of light detected at 480nm decreases significantly. Thus, the relationship between sample concentration and absorbance can be established (the calculation of absorbance refers to the equation (2)). Within the concentration range of (1e-4~1e-7) M, there is a good linear relationship between absorbance and concentration (Fig. 5c, d). Fig. 5e showed the fluorescent images of the sodium fluorescein solutions across orders of concentrations magnitude captured with a digital microscope (it is difficult to distinguish the concentrations from its fluorescence intensity). Therefore, this method could be used to verify the concentration dilution performance of the chip designed in this work.

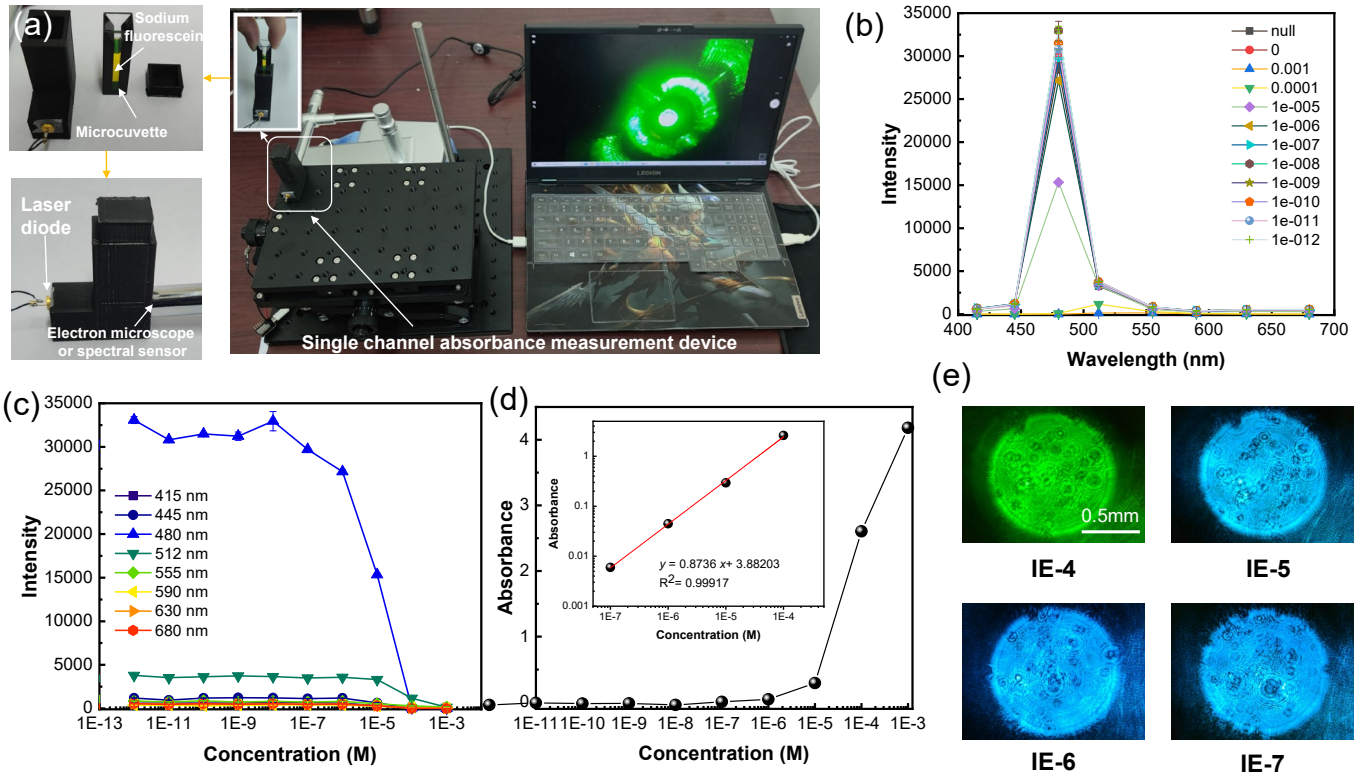

Fig. 5 (a) Absorbance based concentration measurement device, including a 481nm laser light source, a spectrum sensor, a digital microscope and a 3D-printed cuvette holder, and a micro cuvette, computer for spectral sensor data acquisition. (b) Light intensity under laser irradiation with different concentrations of sodium fluorescein. (c) Variation trend of light intensity in 415-680 nm under laser irradiation of sodium fluorescein solutions with different concentrations. (d) Linear relationship between sodium fluorescein concentration and absorbance calculated from absorbance equation (2). (d) Fluorescence images captured by digital microscope under laser irradiation at different concentrations of sodium fluorescein.

According to the absorbance detection device constructed above, five cuvette brackets were constructed by 3D printing at the outlets of the microfluidic dilutor. Micro cuvettes were placed inside the brackets for collecting the products at the outlets in real-time. For each bracket, a 480 nm laser light source and spectral sensor were fixed on both sides of the cuvette. The spectral sensor could be easily disassembled and replaced by a digital microscope for image capture (Fig. 6a). As shown in Fig. 6b, fluorescein sodium at a concentration of 1mM (1e-3) was used as the sample to be diluted, and water was used as the diluent (video 1).

Through the inlet flow rate optimization, when the flow rate ratio of inlet 1: inlet 2: inlet 3 was 100: 900: 850 μL/min, solutions were collected from outlet1-outlet 4, respectively. The absorbance of these solutions indicated that the concentrations basically maintained a linear relationship, and were distributed within four orders of magnitude (According to the linear relationship between concentration and absorbance,

concentration is also distributed within four orders of magnitude) (Fig. 6c). The microfluidic dilutor designed in this work is basically verified to be capable of cross-order sample dilution. The relatively high concentration of outlet 4 may be related to the excessive length of chip design, resulting in slow flow rate of diluent. Therefore, this chip is theoretically suitable for the step-by-step dilution of multistage, but this can only be satisfied when the inlet velocity is very high. In practice, to consider the pressure tolerance of the chip, it is often necessary to select a moderate inlet rate, which may result in the flow reduction or even no product for the last few outlets.

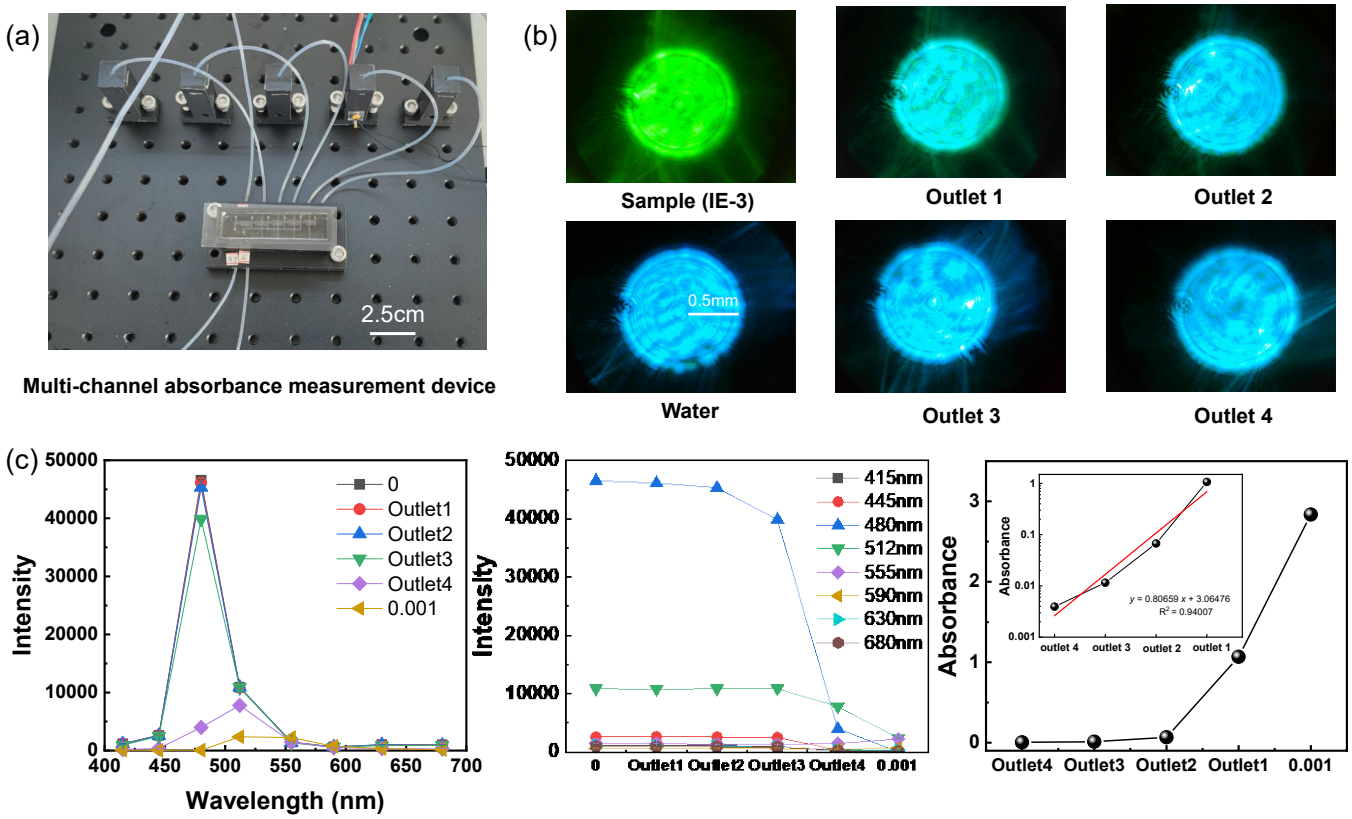

Fig. 6 (a) Absorbance measurement device with the five micro cuvettes for microfluidic dilutor performance verification. (b) Microscopic fluorescent images of fluorescein sodium sample, water, and solutions at the outlet 1-outlet 4. (c) Absorbance of the fluorescein sodium solutions at the outlet 1-outlet 4.

3.3 Tunable liposome nanoparticle synthesis with microfluidic dilutor

To further verify the effectiveness of the microfluidic dilutor design, the chip was used for the preparation of liposome nanoparticles with solvent diffusion method. The experimental setups are shown in Fig. 7a. Soybean lecithin and cholesterol were dissolved in methanol as the sample and water as the diluent. At the beginning, a relatively low flow rate of 30 μl/min was selected for inlet 1 (sample), the flow rate of inlet 2 (diluent) was set 270 μl/min, and the flow rate of inlet 3 (diluent) was set 180 μl/min. According to

the results determined by the laser particle size analyzer, the peak particle size of liposome nanoparticles at outlet 1 was about 140.4 nm, and that at outlet 2 was 198.55nm, while no products were obtained at exit 3-5. As the flow rate of inlet 3 (diluent) increased to 330 μl/min, the product was obtained at outlet 3 (203.7 nm). The peak particle size of outlet 1 and outlet 2 was slightly decreased (134.17 nm and 198.55 nm, respectively) (Fig. 7b, c). According to the effective diameter and polydispersity in Fig. 7e, f, as the flow rate of inlet 3 increased from 180-330 μl/min, the product was obtained at outlet 3, and the size of fabricated lipid nanoparticle was decreased for each outlet, the polydispersity almost remains the same. The farther the outlet from the inlet, the larger the size of the nanoparticles. The preparation principle of liposome nanoparticles adopted is to dissolve lipids in semi-polar methanol solvent to form lipid phase. The mixing of lipid phase and aqueous phase changes the polarity of the solvent to trigger the self-assembly of lipid nanoparticles. The factors affecting the particle size are closely related to the mixing efficiency and speed of lipid phase and water phase. Lipid and water are laminar state in microchannel (means not fully mixed), which only causes moderate solvent polarity changes in lipid phase, with the lipid and water laminar flow into the micromixer with higher mixing efficiency, the water contact with lipid more fully, the solvent polarity changes in lipid phase are stronger. This results in the production of nanoparticles with smaller size. The lower the concentration of liposomes (the higher the dilution degree), that is, the more water phases, the more serious the laminar flow effect between the lipid phase and the water phase, the more difficult it is to mix fully, the less contact between the lipid phase and the water phase. And thus, the slower the polarity change of the solvent, only the nanoparticles with larger size were obtained.

The above two flow rates ratio of inlet 1: inlet 2: inlet 3 (30: 270: 180 μl/min; 30: 270: 330μl/min) respectively were applied to the dilution of 10M FluoresceinIsothiocyanate (FITC) to visualize the entire process, and fluorescence images of microchannel were recorded by an inverted fluorescence microscope, as shown in Fig. 7d. When the flow rate of sample and diluent was 30: 270: 180 μl/min, products were only obtained at the first two outlets, while when the velocity of sample and diluent was 30: 270: 330 μl/min, products were collected at outlet1-outlet 4. The fluorescence intensity is not proportional to the concentration that is consistent with the results in Fig. 4c.

To further verify the tunable performance of the device in the preparation of liposome nanoparticles, the inlet flow rate was increased (60: 540: 600, and 60: 540: 800 μl/min) for lipid nanoparticles fabrication. As shown in Fig. 7g, h, With the overall increase of the three inlet flow rates, the peak particle size of nanoparticles generated at outlet 1 further decreased, and the peak particle size reached 50.6, 80.29, and 100nm, and there were products for all three outlets. But with the increase of the flow rate, two particle size

peaks appeared for outlet 1, indicating that the high flow velocity would cause an unstable influence on the internal flow. But from the effective diameter and polydispersity in Fig. 7i, j, an increase in the overall flow rate will reduce the overall particle size of nanoparticles and still follow the rule that the farther the outlet from the inlet, the larger the size of the nanoparticles. According to the principle of the method adopted in this work, the particle size can be controlled by changing the fluid flow rate and ratio. Therefore, when the concentration of lipid, flow rate and ratio and micro-mixing channel are fixed, the output of nanoparticles is stable. However, in the actual operation process, it is necessary to ensure the orderly switch on the three syringe pumps. In addition, the preservation of the lipid phase solution and the bubbles in the microchannel may affect the stability of the output of nanoparticles. However, the nanoparticle basically remains stable with the trend of the farther the outlet from the inlet, the larger the size of the liposome nanoparticles.

Biological transmission electron microscopy (TEM) was used to observe the morphology of liposome nanoparticles and the encapsulation of liposome vesicles. Since the sizes of nanoparticles prepared at different flow rates are relatively close (between 100-200nm), in order to distinguish them clearly, the liposome solutions obtained at flow rate of 30:270:330 μl/min at outlet 1(Fig. 7k) and 60:540: 800 μl/min at outlet 3 (Fig. 7l) were selected for TEM comparison (DLS peak nanoparticle size were 134.17nm and 241.53nm, respectively). An appropriate amount of liposome nanoparticle solution was dropped onto the copper net covered with carbon film. After being stationary for 2min, the excess liquid was absorbed with filter paper, and then the phosphotungstic acid solution was dropped for negative staining for 2min. The excess liquid was removed and dried at room temperature for observation by TEM. According to the results, the overall particle size observed by TEM was reduced compared with that of DLS, which may be due to the fact that DLS measured the hydration diameter, while TEM measured the dried diameter and clear liposome vesicles could be observed. With the increase of flow rate (Fig. 7l), the particle size of the prepared liposomes increased and the vesicles became more blurred, which be caused by vesicle rupture of liposomes with larger particle size after drying.

The production of liposome nanoparticles could be controlled from two aspects: for the fixed flow rate of inlet 1 and inlet 2, the diluent flow rate (inlet 3) mainly determines the number of outlets that export productions; adjustment of the whole flow rates (inlet1, inlet 2, and inlet 3) mainly determines the nanoparticle size. Dissociable lipids can be protonated under acidic conditions to form cationic lipids, which would bind to negatively charged mRNA by electrostatic action, and form mRNA-loaded lipid nanoparticles. Microfluidic mixing method could be used to produce mRNA-loaded lipid nanoparticles by mixing the lipid solution and mRNA solution in the micromixer. Since lipids are dissolved in ethanol and nucleic acids are dissolved in acid buffer, dialysis or ultrafiltration is required to remove the residual ethanol and replace the

solution system in Phosphate Buffer Saline. Microfluidic dilutor across the order of magnitude has a large adjustment range for the formulation, on the contrary, the adjustment effect may be not obvious for the concentration gradient within one magnitude.

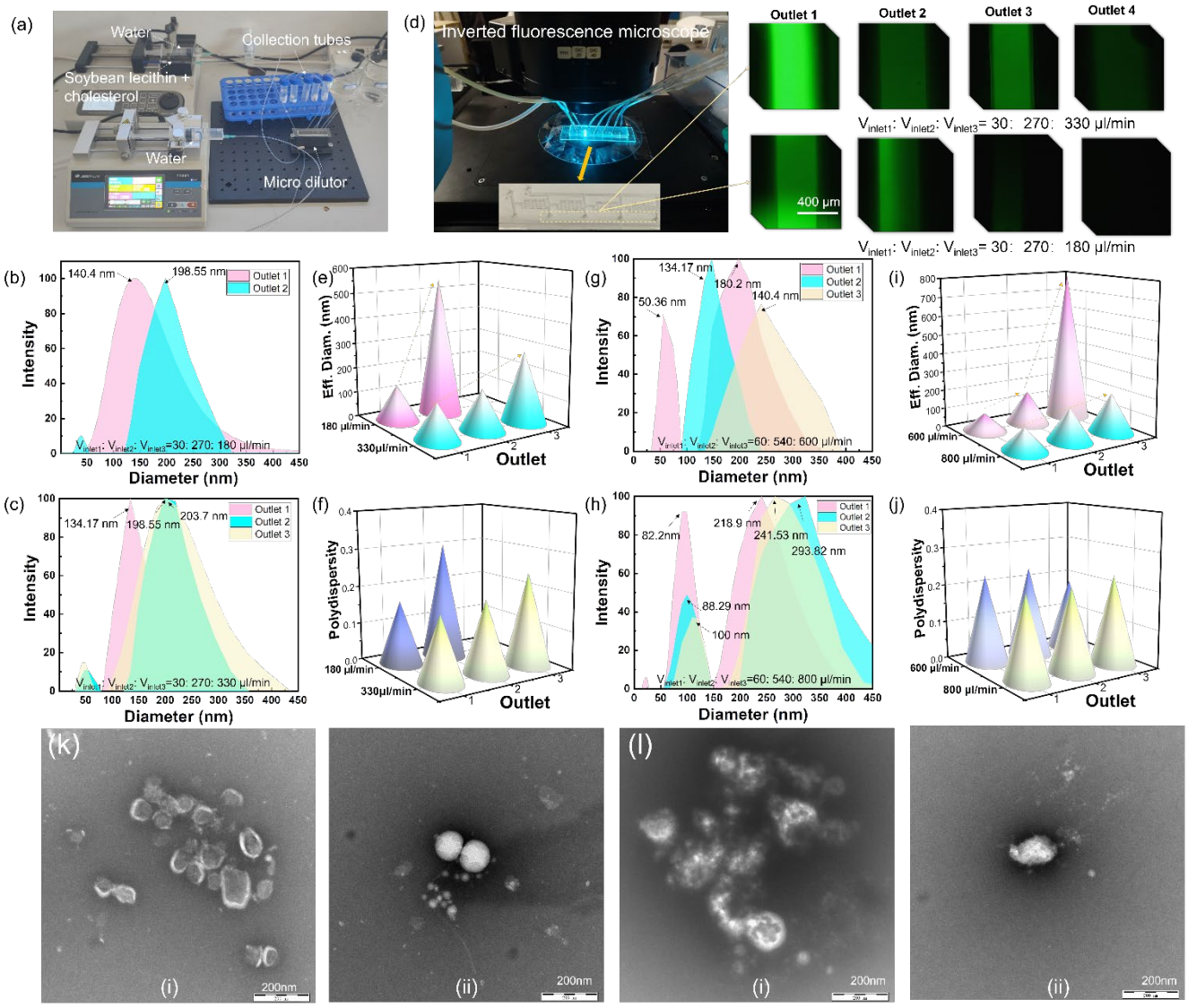

Fig. 7 (a) Experimental setup of tunable synthesis of liposome nanoparticles using the dilution chip. (b, e) Liposome nanoparticle characterization under the flow rates ratio (inlet 1: inlet 2: inlet 3) of 30: 270: 180 μl/min, (c, f) 30: 270: 330 μl/min, (d) FITC fluorescence images of dilutor microchannel recorded by an inverted fluorescence microscope. (g, i) Liposome nanoparticle characterization under the flow rates ratio (inlet 1: inlet 2: inlet 3) of 60: 540: 600 μl/min, (h, j) 60: 540: 800 μl/min. TEM comparison of liposome nanoparticle obtained at flow rate of (k) 30:270:330 μl/min at outlet 1 and (l) 60:540: 800 μl/min at outlet 3.

4. Conclusion

The unequal volume mixing (sample: diluent=1: 9) could be achieved by using the improved serpentine mixing channel. Through the series connection of the structures, the microfluidic dilutor was constructed and could produce a concentration gradient across the order of magnitude verified by the absorbance

measurement device. For concentrations across orders of magnitude, the absorbance of sodium fluorescein was proportional to its concentrations, but not for fluorescent intensity. This microfluidic dilutor can realize the preparation of liposome nanoparticles. The number of outlets that has products and the size of the nanoparticles can be tuned by adjusting the flow rate and flow rate ratio. The design may shed light on the formulation adjustment in the preparation of multi-throughput nanomaterials, especially for large-scale sample preparation.

Acknowledgments

This work was supported financially by the National Natural Science Foundation of China (Grant No. 62101231), the Jiangxi Provincial Natural Science Foundation, China (Grant No. 20202BABL212003), the Hunan Provincial Natural Science Foundation, China (Grant No. 2021JJ40618), the Science and Technology Project of Education Department of Jiangxi Province of China (Grant No. GJJ190510) and PhD Research Startup Fund of Nanchang Hangkong University (EA202008205). The Advantage Subject Team Project of Jiangxi Province (20165BCB19007).

References:

Ahrar, S., Hwang, M., Duncan, P.N., Hui, E.E., 2014. Microfluidic serial dilution ladder. Analyst 139, 187-190.

Avesar, J., Blinder, Y., Aktin, H., Szklanny, A., Rosenfeld, D., Savir, Y., Bercovici, M., Levenberg, S., 2018. Nanoliter Cell Culture Array with Tunable Chemical Gradients. Anal. Chem. 90, 7480-7488.

Baumker, E., Zimmermann, D., Schierle, S., Woias, P., 2021. A Novel Approach to Obtain PAR with a Multi-Channel Spectral Microsensor, Suitable for Sensor Node Integration. Sensors 21, 3390.

Berendsen, J.T.W., Kruit, S.A., Atak, N., Willink, E., Segerink, L.I., 2020. Flow-Free Microfluidic Device for Quantifying Chemotaxis in Spermatozoa. Anal. Chem. 92, 3302-3306.

Chaudhary, N., Weissman, D., Whitehead, K.A., 2021. mRNA vaccines for infectious diseases: principles, delivery and clinical translation. Nat. Rev. Drug Discov. 20, 817-838.

de Almeida, M.S., Susnik, E., Drasler, B., Taladriz-Blanco, P., Petri-Fink, A., Rothen-Rutishauser, B., 2021. Understanding nanoparticle endocytosis to improve targeting strategies in nanomedicine. Chem. Soc. Rev. 50, 5397-5434.

Giorello, A., Minetti, F., Nicastro, A., Berli, C.L.A., 2020. The effect of gravity on microfluidic flow focusing. Sensor. Actuat. B-Chem. 307, 127595.

Gonzalez-Suarez, A.M., Pena-del Castillo, J.G., Hernandez-Cruz, A., Garcia-Cordero, J.L., 2018. Dynamic

Generation of Concentration- and Temporal-Dependent Chemical Signals in an Integrated Microfluidic Device for Single-Cell Analysis. Anal. Chem. 90, 8331-8336.

Horrocks, M.H., Rajah, L., Joensson, P., Kjaergaard, M., Vendruscolo, M., Knowles, T.P.J., Klenerman, D., 2013. Single-Molecule Measurements of Transient Biomolecular Complexes through Microfluidic Dilution. Anal. Chem. 85, 6855-6859.

Hou, X.C., Zaks, T., Langer, R., Dong, Y.Z., 2021. Lipid nanoparticles for mRNA delivery. Nat. Rev. Mater. 6, 1078-1094.

Hu, C., Bai, Y.X., Hou, M., Wang, Y.S., Wang, L.C., Cao, X., Chan, C., Sun, H., Li, W.B., Ge, J., Ren, K.N., 2020. Defect-induced activity enhancement of enzyme-encapsulated metal-organic frameworks revealed in microfluidic gradient mixing synthesis. Sci. Adv. 6, eaax5785.

Jeon, N.L., Dertinger, S.K.W., Chiu, D.T., Choi, I.S., Stroock, A.D., Whitesides, G.M., 2000. Generation of solution and surface gradients using microfluidic systems. Langmuir 16, 8311-8316.

Khoo, B.L., Grenci, G., Lim, Y.B., Lee, S.C., Han, J., Lim, C.T., 2018. Expansion of patient-derived circulating tumor cells from liquid biopsies using a CTC microfluidic culture device. Nat. Protoc. 13, 34-58.

Kim, C., Lee, K., Kim, J.H., Shin, K.S., Lee, K.J., Kim, T.S., Kang, J.Y., 2008. A serial dilution microfluidic device using a ladder network generating logarithmic or linear concentrations. Lab Chip 8, 473-479.

Kim, J., Eygeris, Y., Gupta, M., Sahay, G., 2021. Self-assembled mRNA vaccines. Adv. Drug Deliver. Rev. 170, 83-112.

Kim, T.H., Kim, C.J., Kim, Y., Cho, Y.K., 2018. Centrifugal microfluidic system for a fully automated N-fold serial dilution. Sensor. Actuat. B-Chem. 256, 310-317.

Lee, C.Y., Fu, L.M., 2018. Recent advances and applications of micromixers. Sensor. Actuat. B-Chem. 259, 677-702.

Lim, W., Park, S., 2018. A Microfluidic Spheroid Culture Device with a Concentration Gradient Generator for High-Throughput Screening of Drug Efficacy. Molecules 23, 3355.

Liu, Y., Yang, G.Z., Hui, Y., Ranaweera, S., Zhao, C.X., 2022. Microfluidic Nanoparticles for Drug Delivery. Small, 2106580.

Maeki, M., Kimura, N., Sato, Y., Harashima, H., Tokeshi, M., 2018. Advances in microfluidics for lipid nanoparticles and extracellular vesicles and applications in drug delivery systems. Adv. Drug Deliver. Rev. 128, 84-100.

Prakash, G., Shokr, A., Willemen, N., Bashir, S.M., Shin, S.R., Hassan, S., 2022. Microfluidic fabrication of

lipid nanoparticles for the delivery of nucleic acids. Adv. Drug Deliver. Rev. 184, 114197.

Rismanian, M., Saidi, M.S., Kashaninejad, N., 2019. A new non-dimensional parameter to obtain the minimum mixing length in tree-like concentration gradient generators. Chem. Eng. Sci. 195, 120-126.

Roggo, C., Picioreanu, C., Richard, X., Mazza, C., van Lintel, H., van der Meer, J.R., 2018. Quantitative chemical biosensing by bacterial chemotaxis in microfluidic chips. Environ. Microbiol. 20, 241-258.

Shi, H., Hou, Z., Zhao, Y., Nie, K., Dong, B., Chao, L., Shang, S., Long, M., Liu, Z., 2019a. Rapid and steady concentration gradient generation platform for an antimicrobial susceptibility test. Chem. Eng. J. 359, 1327-1338.

Shi, H.H., Jiang, S.F., Liu, B., Liu, Z.C., Reis, N.M., 2021. Modern microfluidic approaches for determination of ions. Microchem. J. 171, 106845.

Shi, H.H., Nie, K.X., Dong, B., Chao, L.M., Gao, F.X., Ma, M.Y., Long, M.Q., Liu, Z.C., 2020a. Mixing enhancement via a serpentine micromixer for real-time activation of carboxyl. Chem. Eng. J. 392, 123642.

Shi, H.H., Nie, K.X., Dong, B., Long, M.Q., Xu, H., Liu, Z.C., 2019b. Recent progress of microfluidic reactors for biomedical applications. Chem. Eng. J. 361, 635-650.

Shi, H.H., Zhao, Y.L., Liu, Z.C., 2020b. Numerical investigation of the secondary flow effect of lateral structure of micromixing channel on laminar flow. Sensor. Actuat. B-Chem. 321, 128503.

Sugiura, S., Hattori, K., Kanamori, T., 2010. Microfluidic Serial Dilution Cell-Based Assay for Analyzing Drug Dose Response over a Wide Concentration Range. Anal. Chem. 82, 8278-8282.

Sun, S., Liang, N., Yamamoto, H., Kawashima, Y., Cui, F.D., Yan, P.F., 2015. pH-sensitive poly(lactide-co-glycolide) nanoparticle composite microcapsules for oral delivery of insulin. Int. J. Nanomed. 10, 3489-3498.

Suzuki, Y., Onuma, H., Sato, R., Sato, Y., Hashiba, A., Maeki, M., Tokeshi, M., Kayesh, M.E.H., Kohara, M., Tsukiyama-Kohara, K., Harashima, H., 2021. Lipid nanoparticles loaded with ribonucleoprotein-oligonucleotide complexes synthesized using a microfluidic device exhibit robust genome editing and hepatitis B virus inhibition. J. Control. Release 330, 61-71.

Tang, L., He, S., Yin, Y., Liu, H.N., Hu, J.Y., Cheng, J., Wang, W., 2021. Combination of Nanomaterials in Cell-Based Drug Delivery Systems for Cancer Treatment. Pharmaceutics 13, 1888.

Tenchov, R., Bird, R., Curtze, A.E., Zhou, Q.Q., 2021. Lipid Nanoparticles-From Liposomes to mRNA Vaccine Delivery, a Landscape of Research Diversity and Advancement. Acs Nano 15, 16982-17015.

Wan, H., Yin, H.Y., 2018. Tunable and quantitative serial dilution on multi-channel miniaturized

microfluidic electrochemical platform. Sensor. Actuat. B-Chem. 274, 682-688.

Yuan, H., Chen, C.Y., Chai, G.H., Du, Y.Z., Hu, F.Q., 2013. Improved Transport and Absorption through Gastrointestinal Tract by PEGylated Solid Lipid Nanoparticles. Mol. Pharmaceut. 10, 1865-1873.

Zhao, X., Tang, D.Y., Yang, T., Wang, C., 2018. Facile preparation of biocompatible nanostructured lipid carrier with ultra-small size as a tumor-penetration delivery system. Colloid. Surface. B 170, 355-363.

Zijlstra, N., Dingfelder, F., Wunderlich, B., Zosel, F., Benke, S., Nettels, D., Schuler, B., 2017. Rapid Microfluidic Dilution for Single-Molecule Spectroscopy of Low-Affinity Biomolecular Complexes. Angew. Chem. Int. Edit. 56, 7126-7129.